IOP Publishing Semiconductor Science and Technology
Semicond. Sci. Technol. 32 (2017) 065007 (8pp) https://doi.org/10.1088/1361-6641/aa67d7

Group-IV (Si, Ge, and Sn)-doped $AgAlTe_2$ for intermediate band solar cell from first-principles study

Dan Huang[1,2], Jing-Wen Jiang[1], Jin Guo[1,2], Yu-Jun Zhao[3,7], Rongzhen Chen[4,5] and Clas Persson[4,5,6,7]

[1] Guangxi Key Laboratory for Relativistic Astrophysics, Guangxi Colleges and Universities Key Laboratory of Novel Energy Materials and Related Technology, College of Physics Science and Technology, Guangxi University, Nanning 530004, People's Republic of China
[2] Guangxi Collaborative Innovation Center of Structure and Property for New Energy and Materials, School of Material Science and Engineering, Guilin University of Electronic Technology, Guilin, People's Republic of China
[3] Department of Physics and State Key Laboratory of Luminescent Materials and Devices, South China University of Technology, Guangzhou 510640, People's Republic of China
[4] Department of Materials Science and Engineering, Royal Institute of Technology, SE-100 44 Stockholm, Sweden
[5] Centre for Materials Science and Nanotechnology, University of Oslo, PO Box 1048 Blindern, NO-0316 Oslo, Norway
[6] Department of Physics, University of Oslo, PO Box 1048 Blindern, NO-0316 Oslo, Norway

E-mail: zhaoyj@scut.edu.cn and clas.persson@fys.uio.no

Received 15 February 2017, revised 13 March 2017
Accepted for publication 20 March 2017
Published 11 May 2017

Abstract

Earlier studies of chalcopyrites as the absorber for intermediate band solar cells (IBSCs) mainly focused on Cu-based compounds, whose intermediate band is usually empty due to its intrinsic *p*-type conductivity. This is not beneficial to the two sub-bandgap absorptions. In this paper, we demonstrate that the intermediate bands in group IV (Si, Ge, and Sn) doped $AgAlTe_2$ are delocalized and mainly contributed by the anti-bonding state of group-IV elements *s* state and Te-*p* state. Overall, we suggest that Sn-doped $AgAlTe_2$ should be a promising absorber candidate for IBSCs based on the theoretical efficiency and defect stability.

Keywords: intermediate band solar cell, first-principles calculation, electronic structure, defect formation energy, $AgAlTe_2$

(Some figures may appear in colour only in the online journal)

1. Introduction

Thin-film photovoltaic materials have drawn world-wide attention, since converting sunlight into electricity is one of the most promising approaches to solving energy and environmental issues [1]. Chalcopyrite-structure (like $Cu(In,Ga)Se_2$) and its cousin kesterite-structure (like $Cu_2ZnSn(S,Se)_4$) materials as the absorber for the solar cells have been widely studied [2–5]. $Cu(In,Ga)Se_2$ and $Cu_2ZnSn(S,Se)_4$ thin-film photovoltaic devices have achieved a record efficiency of 22.3% [4] and 12.6% [5] on a laboratory scale, respectively. However, a thermodynamic analysis by Shockley and Queisser [6] shows that the efficiency of photovoltaic energy conversion of a single bandgap solar cell is fundamentally limited to 31.0% at 1 sun concentration, because of the broad spectral distribution of solar radiation, limiting the development space of thin-film solar cells. In 1997, the intermediate band solar cell (IBSC) concept [7–11] was proposed to overcome this limit for single bandgap solar cells by making use of below bandgap photons through sequential absorption

[7] Authors to whom any correspondence should be addressed.

processes via an intermediate band (IB). Luque and Martí [7] predicted that the efficiency in the IBSC could increase significantly over the Shockley-Queisser limit to 46.8% at 1 sun and 63.2% at full concentration [12]. The ideal widths of the band gap for the IBSCs are 2.40 and 1.93 eV at 1 sun and full concentration [13, 14], respectively.

Chalcopyrite-structure Cu-based compounds with a suitable band gap (like $CuGaS_2$ [15–27], $CuAlSe_2$ [28], $CuAlS_2$ [29], etc) as the promising host materials for IBSCs have been investigated both theoretically and experimentally. From the experiments, distinct sub-gap absorptions related to the IB have been observed from Fe [15], Cr [16], Ti [17], Ge [18], and Sn [19] doped $CuGaS_2$ samples. The IB positions have been obtained from the absorption spectra measurements. Aguilera *et al* [20] have theoretically investigated the electronic structures and optical properties of $Cu_4TiGa_3S_8$ and $Cu_4CrGa_3S_8$ by generalized gradient approximation (GGA) calculations. Tablero [21] has investigated group-IV (C, Si, Ge, and Sn)-doped $CuGaS_2$ by local-spin density approximation (LDA) calculations. They both found the half-filled IB in the band gap and the increased absorption coefficient at the visible light range in their studied materials. More recently, a hybrid functional like HSE (i.e. Heyd, Scuseria, and Ernzerhof) was used to investigate the electronic structure and optical property of the IB absorber [19, 22–25], with the expectation of a more accurate description for the electronic properties (such as band gap, position of IB, etc) than the traditional LDA or GGA calculations. In fact, Hashemi *et al* [22] found that the earlier reported half-filled IB had turned out to be a lower filled and a higher empty sub-bands in Ti-substituted $CuGaS_2$ after adopting HSE06 functional. Meanwhile, Han *et al* [23] found that unfilled IB appeared in the band gap in Fe- and Co-doped $CuGaS_2$, and Yang *et al* [19] found that there is still a half-filled IB in Sn-doped $CuGaS_2$ from HSE functional calculations. They also pointed out that the transition metal with localized 3*d* states might not be the best candidate to achieve highly efficient IB absorption in chalcopyrite compared to the group-IV element Sn with delocalized 5*s* state. From the electron dispersion point of view, the group-IV elements (Si, Ge, and Sn) are promising dopant candidates for IBSCs. In order to obtain IBs in the gap, a large doping concentration is needed. In addition to electronic structure and optical property investigations, the free energy of formation and the allowed chemical potential derived from first-principles calculations have been used to theoretically evaluate the possibility of doping concentration. From the investigation on the free energy of formation of the materials, Palacios *et al* [26] found that the substitution by Cr or Ti at Ga sites in $CuGaS_2$ is energetically unfavorable, indicating that preparation methods controlled by kinetics must be used to obtain large dopant concentrations. To avoid the formation of impurities containing the doping elements, Tablero *et al* [27] found that some of the elements (i.e. Fe, Co, Ni, Pd, Rh, Ir, Si, Ge, and Sn) can be soluble in $CuGaS_2$ and are suggested as possible dopant candidates. Of note is that they did not calculate the specific defect formation energies to find out the suitable doping element in detail.

As an absorber for the solar cell, Ag-based compounds have been paid much less attention than the Cu-based compounds. Some of the Ag-based compounds (like $AgInSe_2$ [30, 31], $AgGaTe_2$ [32, 33], $AgAlTe_2$ [34], $Ag_2ZnSnSe_4$ [35], etc) have been reported for application on solar cells. On the other hand, Ag-based compounds have their unique properties with respect to the Cu-based compounds. Ag-based compounds generally have lower valence band position than Cu-based compounds [36, 37], implying that they are easier to be *n*-type. For example, Yuan *et al* [38] found from the first-principles study that the *p*-type defect Ag vacancy (V_{Ag}) in Ag_2ZnSnS_4 has much higher formation energy than Cu vacancy (V_{Cu}) in Cu_2CdSnS_4 and Cu_2ZnSnS_4. Experimentally, *n*-type conductivity has been reported in $AgInSe_2$ [31] and $Ag_2ZnSnSe_4$ [35]. Owing to the half-filled property required for IBs [39, 40], the *p*-type conductivity in Cu-based compounds may lead to empty IB and this is destructive to the half-filled character of IB. Therefore, from the type of conductivity point of view, Ag-based compounds with a proper band gap may be more suitable as the host materials for IBSCs. In addition, Ag-based chalcopyrite-type nanoparticles can be synthesized easily under milder reaction conditions than those of Cu-based ones [41]. Although Cu is cheaper and more abundant than Ag, Ag is advantageous with respect to In and Ga based on earth abundance and cost [42]. The inclusion of Ag in the thin film would not impose a large increase on the eventual cost of the solar panels [42]. For tellurium, although it is rare in the Earth's crust and abundant in the universe, the CdTe module production cost in 2010 was one of the lowest in the photovoltaic industry [43]. With improved recycling techniques [44], the supply of Te will not be a major problem in the near future. The chalcopyrite $AgAlTe_2$ with a band gap of 2.27 eV [45] has been investigated as the absorber for solar cells [34, 45] and the photocatalyst for water splitting [46]. Its band gap is close to the ideal width (2.4 eV) for IBSCs at 1 sun concentration. Therefore, $AgAlTe_2$ can be regarded as a promising host material for IBSCs.

In this paper, group-IV (Si, Ge, and Sn)-doped $AgAlTe_2$ as an absorber for IBSCs has been investigated by first-principles study based on HSE hybrid functional. Our results reveal that the IBs are dominated by the anti-bonding state of group-IV elements *s* state and Te-*p* state, which are more delocalized than that from transition metal-doped chalcopyrite compounds. Based on the bond length and atomic orbital energy, we have explained the sequence of IBs in (Si, Ge, and Sn)-doped $AgAlTe_2$. We also discuss the theoretical efficiency according to the width of sub-band gaps and evaluated the difficulty of doping to a large concentration based on the calculated defect formation energy. Our results show that Sn doping at the Al site in $AgAlTe_2$ has low formation energy under Te-rich condition and can produce the desired sub-band gaps for IBSCs.

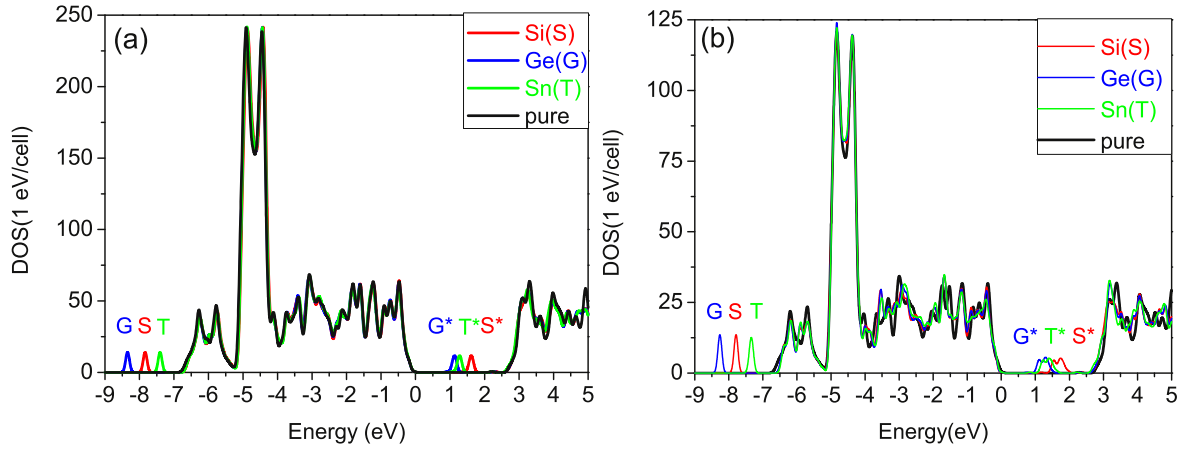

Figure 1. The total DOS of pure and (Si, Ge, and Sn)-doped $AgAlTe_2$ from 64-atom supercells (a) and 32-atom supercells (b). The average potentials of host elements far away from the dopant are used to align the DOS. The valence band maximum of the pure $AgAlTe_2$ is set to zero.

2. Computational details

All calculations were carried out by the density functional approach in the VASP package [47] with plane-wave basis to describe the valence states. To describe the interactions between the valence electrons (Ag: $4d^{10}5s^1$, Al: $3s^23p^1$, Te: $5s^25p^4$, Si: $3s^23p^2$, Ge: $4s^24p^2$, Sn: $5s^25p^2$) and the core, the projector augmented-wave implementation was used [48]. The calculations were performed using the screened hybrid exchange–correlation functional [49] developed by Heyd, Scuseria, and Ernzerhof. The cutoff energy for the plane-wave basis is set to 400 eV for all the calculations. In order to determine the IB position in the band gap without correction, the percentage of the exact non-local Fock exchange is adjusted to 30% to meet the accurate band gap of $AgAlTe_2$ from the experiment [45]. Our calculated crystal parameters for intrinsic $AgAlTe_2$ are $a = b = 6.38$ Å, $c = 12.11$ Å, $c/2a = 0.95$, and $u = 0.27$, in line with the experimental observations [50] ($a = b = 6.30$ Å, $c = 11.83$ Å, $c/2a = 0.94$, and $u = 0.26$). For the calculations on systems containing defects, $\sqrt{2} \times \sqrt{2} \times 1$ supercells containing 32 atoms (doping concentration at 12.5%) and $2 \times 2 \times 1$ supercells containing 64 atoms (doping concentration at 6.25%) are adopted. For the calculation on defect formation energy, we used the supercells containing 64 atoms. All the atoms are fully relaxed throughout this work with the Γ-centered k-point mesh [51] of a reciprocal space discretization of ~ 0.26 Å^{-1}. After the structure relaxation, a denser Γ-centered k-mesh with a reciprocal space discretization of ~ 0.17 Å^{-1} is used for the electronic structures and optical properties calculations.

3. Results and discussions

3.1. Analysis on density of states (DOS) and the sequence of the IBs

Figures 1(a) and (b) show the total DOS of the pure and (Si, Ge, and Sn)-doped $AgAlTe_2$ from 64-atom supercells and 32-atom supercells. We find that the DOS of the valence and conduction bands do not show a significant change with and without doping. With Si, Ge, or Sn doped at the Al site in $AgAlTe_2$, two series of additional peaks appear in the DOS. The first series of additional peaks (impurity peak I) are around the energy range from −8.5 to −7.2 eV in the sequence of Ge < Si < Sn. Another series of additional peaks (impurity peak II) are in the band gap, forming the IBs. The sequence of the IBs is Ge < Sn < Si. Since the two sub-gap absorptions are related to the position of the IB, it is important to understand the physics of the sequence, which has a critical impact on the theoretical efficiency of the doped systems.

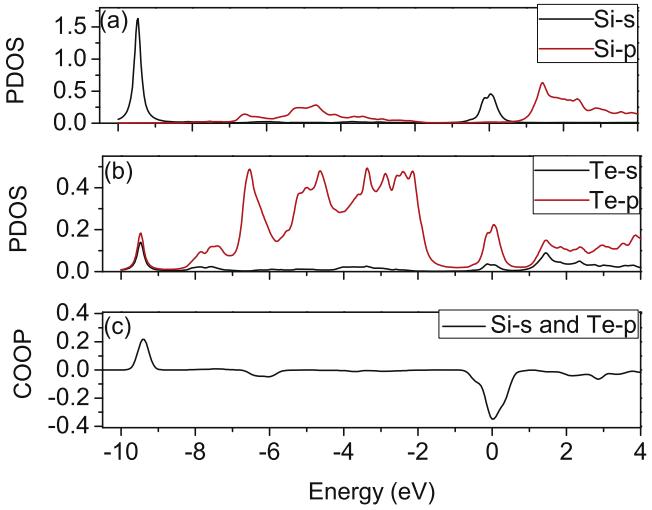

Figure 2. PDOS of Si(a) and Te(b) and the COOP(c) between Si-*s* and Te-*p* in Si-doped $AgAlTe_2$. Fermi energy level is set to zero.

The partial DOS (PDOS) of Si and Te in Si-doped $AgAlTe_2$ from 32-atom supercells are shown in figures 2(a) and (b), from which we note that the IB (i.e. impurity peak II) mainly comes from the Si-*s* and Te-*p* states. In addition, impurity peak I is also composed of Si-*s* state and Te-*p* state. To identify the bonding character of Si and Te, we have plotted their crystal orbital overlap populations (COOPs, see figure 2(c)), which are

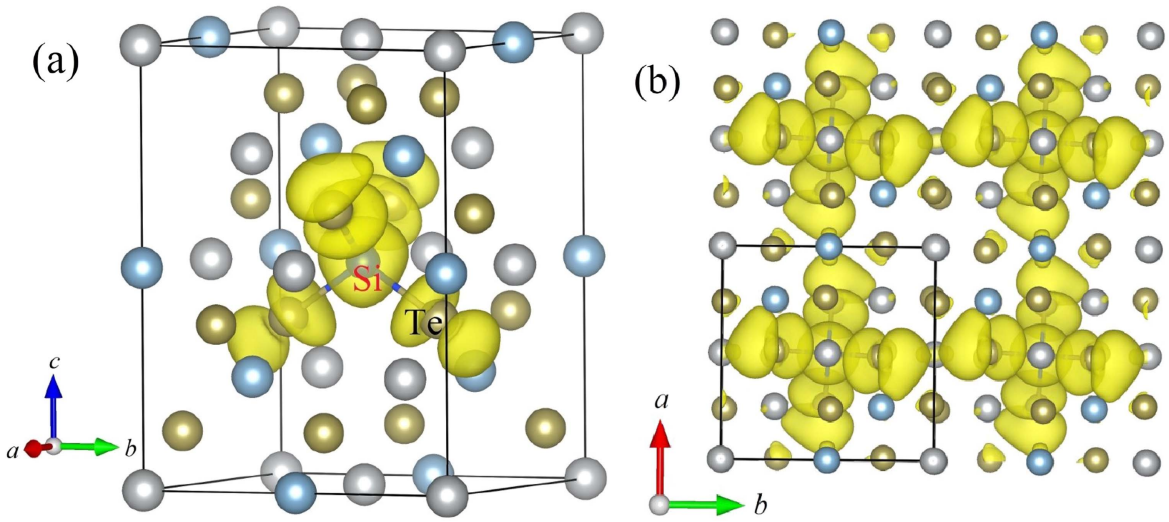

Figure 3. Wave function square of the IB in Si-doped $AgAlTe_2$. Densities are at 0.002 e/Å^3(a) and 0.001 e/Å^3(b), respectively.

computed using the Lobster program developed by Dronskowski and co-workers [52, 53]. The COOPs add the overlap dimension by showing the bonding (COOP $>$ 0), non-bonding (COOP $=$ 0), or anti-bonding (COOP $<$ 0) character of each electronic state over the system's chemical bonds. Combining the COOPs and PDOS, we can understand that impurity peak I at around -9 eV comes from the bonding state of Si-*s* state and Te-*p* state and the IB (i.e. impurity peak II) in the band gap comes from the anti-bonding state of Si-*s* state and Te-*p* state. The wave function square (see figure 3(a)) of the IB in Si-doped $AgAlTe_2$ also shows anti-bonding character, consistent with the bonding analysis of COOPs.

For Ge and Sn-doped $AgAlTe_2$, the PDOS and bonding characters are similar to those of Si-doped $AgAlTe_2$. The atomic orbital energies [54] of Si-3*s*, Ge-4*s,* and Sn-5*s* are -10.83, -11.61, and -10.05 eV, respectively. Consequently, the sequence of the energies of the outside *s*-electrons is Ge $<$ Si $<$ Sn, which is displayed in the left of figure 4. The atomic orbital energy [54] of Te-5*p* is -6.17 eV, which is presented in the right of figure 4. Besides the atomic orbital energy, the interactions between group-IV elements and Te are influenced by the bond lengths. The calculated bond lengths of Si-Te, Ge-Te, and Sn-Te in doped 32-atom supercells are 2.67, 2.73, and 2.90 Å, respectively. Figure 4 shows the schematic diagram of the bonding/anti-bonding interactions between group-IV elements and Te in (Si, Ge, and Sn)-doped $AgAlTe_2$. Based on the atomic orbital energies and bond lengths, we can understand the sequence of the impurity peaks that appeared in the DOS (figure 1). Since Sn-*s* state has the highest atomic orbital energy and longest bond length, the bonding state of Sn-*s* and Te-*p* is at the highest position among all bonding states. Owing to the shortest bond length of Si and Te and the mediate atomic orbital energy of Si-*s* state, the anti-bonding state of Si-*s* and Te-*p* is pushed to the highest position among all anti-bonding states. Due to the lowest atomic orbital energy of Ge-*s* and the mediate bond length of Ge and Te, the bonding/anti-bonding states of Ge-*s* and Te-*p* still stay at the lowest positions among

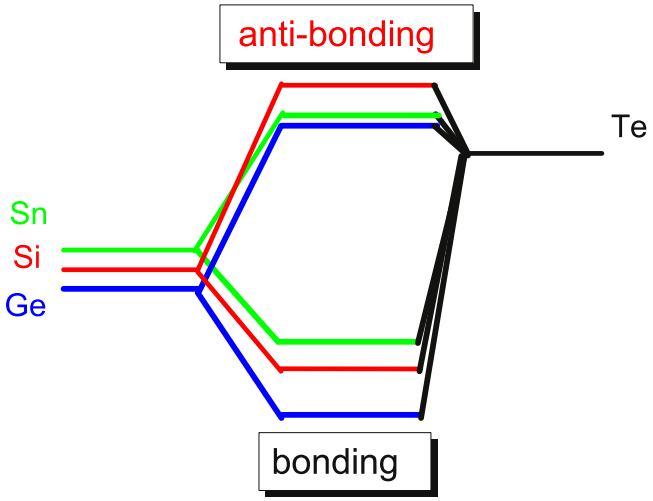

Figure 4. Schematic diagram of the bonding/anti-bonding interactions of group-IV elements and Te in (Si, Ge, and Sn)-doped $AgAlTe_2$.

all the bonding/anti-bonding states. Owing to the IB positions related to the sub-bandgap absorption, the bonding analysis can provide a way to find a suitable dopant for the absorber of IBSCs.

3.2. Width of IBs at concentrations of 6.25% and 12.5%

When the doping concentration increases in $AgAlTe_2$, the original band gap and width of the IB are expected to change correspondingly. We have calculated the band offsets among the pure and doped systems with different dopants for two different concentrations. The band offset was calculated with the conventional approach [55], i.e. aligned by the average potentials of host elements far away from the dopant. Figure 5(a) presents the band offsets and schematic band structures for pure $AgAlTe_2$ and (Si, Ge, and Sn)-doped $AgAlTe_2$ at two different doping concentrations. As shown in the calculated band structures in figure 5(b), the IBs in (Si, Ge, and Sn)-doped $AgAlTe_2$ at 12.5% concentration have a

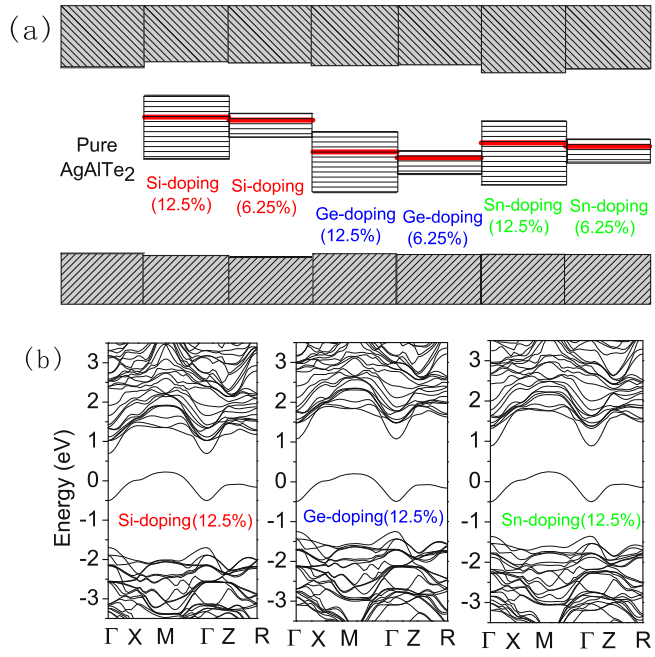

Figure 5. Band offsets and schematic band structures (a) for pure $AgAlTe_2$ and group-IV (Si, Ge, and Sn)-doped $AgAlTe_2$ at concentrations of 6.25% and 12.5%. The red lines in the IBs denote the calculated Fermi level on the ideal (Si, Ge, and Sn)-doped $AgAlTe_2$ systems. HSE-calculated band structure (b) of the (Si, Ge, and Sn)-doped $AgAlTe_2$ at 12.5% concentration. Fermi energy level of each system is set to zero in figure 5(b).

similar shape and delocalized characteristic, while their positions shift from each other in the band gap. The width of the band gaps and IBs are listed in table 1. The original band gaps and the band edge positions are slightly influenced by doping. As expected, the width of the IBs broadens with the increase of doping concentration. The width of the IBs increases from ~0.27–0.29 eV at 6.25% doping concentration to ~0.75–0.78 eV at 12.5%, which is wider than those of the impurity bands from the transition metal-doped chalcopyrite compounds (like $CuGaS_2$:Ti [22], $CuGaS_2$:Fe [24], $CuAlSe_2$:Ti [28], etc) at the corresponding doping concentrations. The delocalized characters (see figure 3(b)) of the IBs in (Si, Ge, and Sn)-doped $AgAlTe_2$ are originally from the group-IV *s* states and Te-*p* states. Owing to the delocalized electronic structure of IBs, the generated carriers can transport freely and then overcome the non-radiative recombination [40, 56]. In addition, the impurity bands in transition metal-doped chalcopyrite compounds are fully-filled or empty from previous HSE calculations [22, 23], which cannot serve the two-step jumping of an electron. The half-filled and delocalized properties of the IB of (Si, Ge, and Sn)-doped $AgAlTe_2$ make them promising candidates for IBSCs. The Fermi energy levels in figure 5 (i.e. the red lines) are obtained from the calculations from the ideal (Si, Ge, and Sn)-doped $AgAlTe_2$ systems. All of the calculated Fermi energy levels stay at the n-type region and may not be alternated by the intrinsic defects in heavily (Si, Ge, and Sn)-doped samples. Moreover, it is easier for $AgAlTe_2$ to maintain the Fermi level at the *n*-type region to keep the IB half-filled than Cu-based chalcopyrite compounds [35, 38]. Of note is that only neutral substituting defects of group IV at the Al site are considered for the calculated Fermi level (cf. figure 5), as the ionization is unlikely for the impurities with deep levels, and the influence of the intrinsic defects could be neglected with respect to the high concentration of group IV dopants.

3.3. Theoretical efficiency

Figure 6 presents the absorption coefficient of pure $AgAlTe_2$ and (Si, Ge, and Sn)-doped $AgAlTe_2$ at doping concentrations of 6.25% and 12.5%. Obviously, the capabilities of light absorption have been enhanced for the doped systems under the solar radiation spectrum by the sub-bandgap absorption. With the doping concentration increases from 6.25% to 12.5%, the absorption coefficient is also improved. Based on the width of the band gap and the sub-band gap listed in table 1 and not involving the calculated optical absorption spectra, we simply estimate the maximum theoretical efficiency at 1 sun concentration of each of our studied materials. Owing to the similar width of the two sub-band gaps (for example, 1.19 and 1.14 eV for Ge doping at 6.25% concentration), Ge-doped $AgAlTe_2$ has the lowest theoretical efficiency among the (Si, Ge, and Sn)-doped $AgAlTe_2$. For Si- and Sn-doped $AgAlTe_2$, the theoretical efficiency at 1 sun concentration can increase to ~40% owing to the appropriate sub-band gaps. Especially for Sn doping at 12.5% concentration, the theoretical efficiency can reach 45%, which is close to the maximum theoretical efficiency (46.8%) of an absorber with one IB at 1 sun concentration [12]. Here, we point out that Yu and Zunger [57] have considered the optical absorption spectra and then the depth of the absorber to study the theoretical efficiency of a lot of chalcopyrite materials with a single band gap. Over 20 compounds with high spectroscopic limited maximum efficiency have been selected from around 260 generalized $I_pIII_qVI_r$ chalcopyrite materials.

3.4. Defect formation energy and possible doping concentration

In order to obtain an IB, as discussed in the above subsection, other than impurity level in the doped systems, the samples generally need to contain dopants with a large concentration. To evaluate the possibility of reaching a large concentration of group-IV dopants in $AgAlTe_2$, we have calculated the defect formation energy [58] according to:

$$\Delta E(D^0) = E(D^0) - E(0) + \sum_{\alpha} n_{\alpha}(\Delta\mu_{\alpha} + \mu_{\alpha}^{\text{solid}}) \quad (1)$$

where $E(D^0)$ and $E(0)$ are the total energies of the supercells with and without defects. Here, $(\Delta\mu_{\alpha} + \mu_{\alpha}^{\text{solid}})$ is the absolute value of the chemical potential of atom α, and $\mu_{\alpha}^{\text{solid}}$ is defined as the chemical potential of the elemental solid. Also, n_{α} is the number of atoms related to the defect; $n_{\alpha} = -1$ if an atom is added, while $n_{\alpha} = 1$ if an atom is removed.

Table 1. Widths of the band gap, sub-gap, and IB (in eV), as well as the theoretical efficiency at 1 sun concentration in pure $AgAlTe_2$ and (Si, Ge, and Sn)-doped $AgAlTe_2$ at doping concentrations of 6.25% and 12.5%.

Systems	Band gap	Sub-gap1 (VBM-Fermi)	Sub-gap2 (Fermi-CBM)	Width of IB	Theo. efficiency
Pure $AgAlTe_2$	2.27				23%
Si (12.5%)	2.39	1.70	0.69	0.78	38%
Si (6.25%)	2.38	1.68	0.70	0.29	39%
Ge (12.5%)	2.33	1.26	1.07	0.75	33%
Ge (6.25%)	2.33	1.19	1.14	0.27	24%
Sn (12.5%)	2.24	1.37	0.87	0.78	45%
Sn (6.25%)	2.29	1.34	0.95	0.28	41%

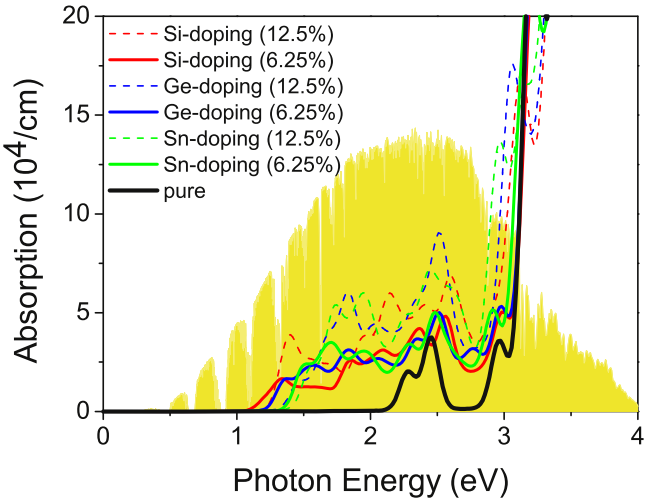

Figure 6. Absorption coefficient of pure $AgAlTe_2$ and (Si, Ge, and Sn)-doped $AgAlTe_2$ with two different concentrations. The reference air-mass 1.5-solar spectral irradiance is plotted in yellow.

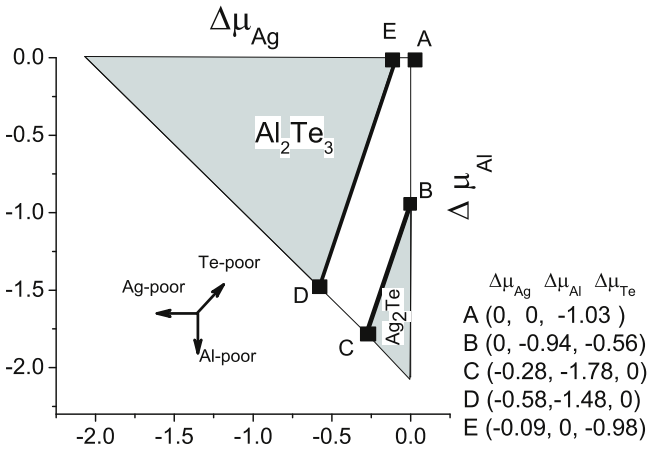

Figure 7. Allowed chemical potential ranges (white area in the triangle) for a stable $AgAlTe_2$ with consideration of competing compounds. Points A, B, C, D, and E represent five extreme conditions considered in this work.

The chemical potentials of each constituent species ($\Delta\mu_\alpha$) can be varied to reflect specific equilibrium growth conditions, but their summation is always equal to the calculated formation enthalpy of $AgAlTe_2$ in order to maintain the stability of the host:

$$\Delta\mu_{Ag} + \Delta\mu_{Al} + 2\Delta\mu_{Te} = \Delta H(AgAlTe_2) = -2.06\ \text{eV}. \quad (2)$$

In addition to the host stability condition, the atomic chemical potentials should be smaller than that of the corresponding elemental solid in order to avoid precipitation of elemental solids:

$$\Delta\mu_{Ag} \leqslant 0,\ \Delta\mu_{Al} \leqslant 0,\ \Delta\mu_{Te} \leqslant 0. \quad (3)$$

The chemical potentials are further restricted by the competing compounds. These crucial constraints are listed as the following:

$$2\Delta\mu_{Al} + 3\Delta\mu_{Te} \leqslant \Delta H(Al_2Te_3) = -2.96\ \text{eV}. \quad (4)$$

$$2\Delta\mu_{Ag} + \Delta\mu_{Te} \leqslant \Delta H(Ag_2Te) = -0.56\ \text{eV}. \quad (5)$$

Figure 7 shows the calculated chemical potential domains for $AgAlTe_2$. From the constraints imposed by the competing compounds, the white areas in the triangle are the allowed chemical potential ranges for $AgAlTe_2$. Within this boundary, we explicitly consider five extreme growth conditions. The detailed values of the chemical potentials of Ag, Al, and Te under different growth conditions are shown in figure 7. The maximum allowed values of the chemical potentials for Si, Ge, and Sn are used for the defect formation calculations, with the following constraints: $2\Delta\mu_{Si} + 3\Delta\mu_{Te} \leqslant \Delta H(Si_2Te_3) = -0.80\ \text{eV}$, $\Delta\mu_{Ge} + \Delta\mu_{Te} \leqslant \Delta H(GeTe) = -0.20\ \text{eV}$, $\Delta\mu_{Sn} + \Delta\mu_{Te} \leqslant \Delta H(SnTe) = -0.15\ \text{eV}$. Here, the experimental data of the formation enthalpies of Si_2Te_3 [59], GeTe [60], and SnTe [61] are adopted.

Figure 8 shows the formation energies of Si, Ge, and Sn substituting at the Al site in $AgAlTe_2$ under various chemical potential conditions. We find that Sn doping always has the lowest formation energy compared to Si and Ge doping when adopting elemental solids as the dopant sources. This could be attributed to the strong covalent bonding in elemental Si and Ge bulks, and a relatively weaker metallic bond in bulk Sn. Taking out an atom from the pristine crystal Si and Ge and then doping at the Al site in $AgAlTe_2$ may need to consume more energy than that from the pristine crystal Sn, as supported by the corresponding cohesive energies of elemental

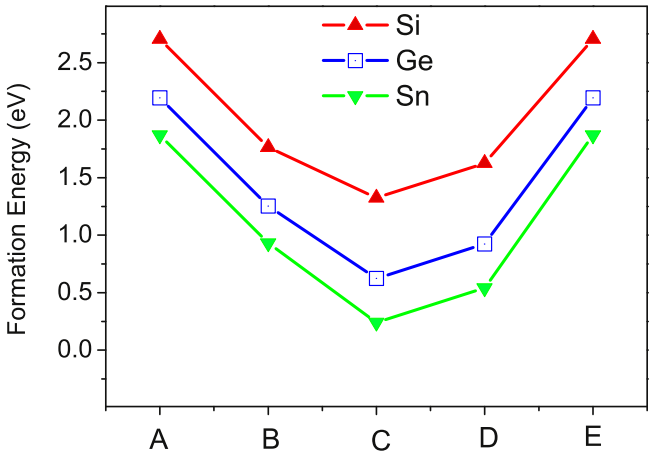

Figure 8. Formation energies of Si, Ge, and Sn substituting at the Al site in $AgAlTe_2$ as a function of the chemical potential at points A, B, C, D, and E shown in figure 7.

Si, Ge, and Sn bulks [62] of 4.63, 3.85, and 3.14 eV/atom, respectively. The defect formation energy of Sn_{Al} can reach 0.24 eV under point C (i.e. Te-rich condition), which implies that Sn_{Al} can reach a large doping concentration. Using the Boltzmann distribution law and assuming the growth temperature T of 1000 K [34], the Sn_{Al} doping concentration can reach ~6% under Te-rich condition. As previously mentioned, our calculated defect formation energies are based on using the elemental solid as the dopant source under equilibrium condition. By using other dopant sources [63] (like SiH_4, GeH_4, etc) and the non-equilibrium growth method [64], the doping concentration may further increase in Si- or Ge-doped $AgAlTe_2$ to exceed the limit of the equilibrium doping. These methods can also be utilized to achieve a large Sn doping concentration. Combining the theoretical efficiency and defect formation energy, we suggest that Sn-doped $AgAlTe_2$ can realize a large doping concentration easily and possess a desired theoretical efficiency, which should make it a promising absorber candidate for IBSCs.

4. Conclusion

In summary, we have studied the (Si, Ge, and Sn)-doped $AgAlTe_2$ as an absorber for IBSCs by HSE hybrid functional calculations. We demonstrate that all the studied dopants can induce a delocalized IB in $AgAlTe_2$, dominated by the anti-bonding state of group-IV element *s* and Te-*p* states. The energy sequence of the IB positions in the band gap is Ge < Sn < Si, which is explained by a simple model with the bond lengths and atomic orbital energies. Based on the width of the sub-band gap and the defect formation energy, we have evaluated the theoretical efficiency and the possibility of doping with a high concentration. This suggests that Sn-doped $AgAlTe_2$ can achieve a high theoretical efficiency with a high doping concentration, which should make it a promising absorber for IBSCs.

Acknowledgments

This work was financially supported by the National Natural Science Foundation of China (Grant Nos. 61664003, 51571065, and 11574088), the Natural Science Foundation of Guangxi Province (Grant No. 2014GXNSFCA118002), the Scientific Research Foundation of Guangxi University (Grant No. XGZ130718), and the Research Council of Norway (Grant No. 243642). The authors acknowledge PRACE awarding access to the resource MareNostrum based in Spain at BSC-CNS.

References

[1] Polman A, Knight M, Garnett E C, Ehrler B and Sinke W C 2016 *Science* **352** aad4424
[2] Contreras M A, Egaas B, Ramanathan K, Hiltner J, Swartzlander A, Hasoon F and Noufi R 1999 *Prog. Photovoltaics* **7** 311
[3] Todorov T K, Tang J, Bag S, Gunawan O, Gokmen T, Zhu Y and Mitzi D B 2013 *Adv. Energy Mater.* **3** 34
[4] Jackson P, Wuerz R, Hariskos D, Lotter E, Witte W and Powalla M 2016 *Phys. Status Solidi-Rapid Res. Lett.* **10** 583
[5] Wang W, Winkler M T, Gunawan O, Gokmen T, Todorov T K, Zhu Y and Mitzi D B 2014 *Adv. Energy Mater.* **4** 1301465
[6] Shockley W and Queisser H J 1961 *J. Appl. Phys.* **32** 510
[7] Luque A and Martí A 1997 *Phys. Rev. Lett.* **78** 5014
[8] Luque A, Martí A and Stanley C 2012 *Nat. Photon.* **6** 146
[9] Okada Y *et al* 2015 *Appl. Phys. Rev.* **2** 021302
[10] Flores M A, Menéndez-Proupin E, Orellana W and Peña J L 2016 *J. Phys. D.: Appl. Phys.* **50** 035501
[11] Yassin O A 2015 *J. Phys. D.: Appl. Phys.* **48** 355106
[12] Brown A S and Green M A 2002 *J. Appl. Phys.* **92** 1329
[13] Ley M, Boudaden J and Kuznicki Z T 2005 *J. Appl. Phys.* **98** 044905
[14] Wang W, Lin A S and Phillips J D 2009 *Appl. Phys. Lett.* **95** 011103
[15] Marsen B, Klemz S, Unold T and Schock H W 2012 *Prog. Photovoltaics* **20** 625
[16] Chen P, Qin M, Chen H, Yang C, Wang Y and Huang F 2013 *Phys. Status Solidi* . A **210** 1098
[17] Lv X, Yang S, Li M, Li H, Yi J, Wang M, Niu G and Zhong J 2014 *Sol. Energy* **103** 480
[18] Qin M S, Huang F Q and Chen P 2012 *Appl. Mech. Mater.* **148** 1558
[19] Yang C, Qin M, Wang Y, Wan D, Huang F and Lin J 2013 *Sci. Rep.* **3** 1286
[20] Aguilera I, Palacios P and Wahnón P 2010 *Sol. Energy Mater. Sol. Cells* **94** 1903
[21] Tablero C 2010 *Thin Solid Films* **519** 1435
[22] Hashemi J, Akbari A, Huotari S and Hakala M 2014 *Phys. Rev.* B **90** 075154
[23] Han M, Zhang X and Zeng Z 2014 *RSC Adv.* **4** 62380
[24] Koskelo J, Hashemi J, Huotari S and Hakala M 2016 *Phys. Rev.* B **93** 165204
[25] Han M, Zhang X, Zhang Y and Zeng Z 2016 *Sol. Energy Mater. Sol. Cells* **144** 664
[26] Tablero C and Fuertes Marrón D 2010 *J. Phys. Chem.* C **114** 2756
[27] Palacios P, Aguilera I, Wahnón P and Conesa J C 2008 *J. Phys. Chem.* C **112** 9525
[28] Wang T, Li X, Li W, Huang L, Ma C, Cheng Y, Cui J, Luo H, Zhong G and Yang C 2016 *Mater. Res. Express* **3** 045905

[29] Guo C, Yang C, Xie Y, Chen P, Qin M, Huang R and Huang F 2016 *RSC Adv.* **6** 40806
[30] Mustafa H, Hunter D, Pradhan A K, Roy U N, Cui Y and Burger A 2007 *Thin Solid Films* **515** 7001
[31] Jacob R, Okram G S, Naduvath J, Mallick S and Philip R R 2015 *J. Phys. Chem.* C **119** 5727
[32] Krustok J, Jagomägi A, Grossberg M, Raudoja J and Danilson M 2006 *Sol. Energy Mater. Sol. Cells* **90** 1973
[33] Kumar R and Bedi R K 2005 *J. Mater. Sci.* **40** 455
[34] Uruno A, Usui A and Kobayashi M 2014 *J. Electron. Mater.* **43** 2874
[35] Gershon T, Sardashti K, Gunawan O, Mankad R, Singh S, Lee Y S, Ott J A, Kummel A and Haight R 2016 *Adv. Energy Mater.* **6** 1601182
[36] Huang D and Persson C 2014 *Chem. Phys. Lett.* **591** 189
[37] Yuan Z K, Chen S, Xiang H, Gong X G, Walsh A, Park J S, Repins I and Wei S H 2015 *Adv. Funct. Mater.* **25** 6733
[38] Zhang S B, Wei S H and Zunger A 2000 *Phys. Rev. Lett.* **84** 1232
[39] Luque A and Marti A 2001 *Prog. Photovoltaics* **9** 73
[40] Zhang J, He H and Pan B 2015 *Nanotechnology* **26** 195401
[41] Torimoto T, Kameyama T and Kuwabata S 2014 *J. Phys. Chem. Lett.* **5** 336
[42] Chagarov E, Sardashti K, Kummel A C, Lee Y S, Haight R and Gershon T S 2016 *J. Chem. Phys.* **144** 104704
[43] Zweibel K 2010 *Science* **328** 69
[44] Redlinger M, Eggert R and Woodhouse M 2015 *Sol. Energy Mater. Sol. Cells* **138** 58
[45] Uruno A, Takeda Y, Inoue T and Kobayashi M 2016 *Phys. Status Solidi.* C **13** 413
[46] Huang D, Ju Z, Ning H, Li C, Yao C and Guo J 2014 *Mater. Chem. Phys.* **148** 882
[47] Kresse G and Hafner J 1993 *Phys. Rev.* B **47** 558
[48] Kresse G and Joubert D 1999 *Phys. Rev.* B **59** 1758
[49] Heyd J, Peralta J E, Scuseria G E and Martin R L 2005 *J. Chem. Phys.* **123** 174101
[50] Tell B, Shay J L and Kasper H M 1974 *Phys. Rev.* B **9** 5203
[51] Monkhorst H J and Pack J D 1976 *Phys. Rev.* B **13** 5188
[52] Maintz S, Deringer V L, Tchougréeff A L and Dronskowski R 2013 *J. Comput. Chem.* **34** 255
[53] Dronskowski R and Bloechl P E 1993 *J. Phys. Chem.* **97** 8617
[54] Kotochigova S, Levine Z H, Shirley E L, Stiles M D and Clark C W 1997 *Phys. Rev.* B **55** 191
[55] Gai Y, Li J, Li S S, Xia J B and Wei S H 2009 *Phys. Rev. Lett.* **102** 036402
[56] Luque A, Martí A, Antolín E and Tablero C 2006 *Physica* B **382** 320
[57] Yu L and Zunger A 2012 *Phys. Rev. Lett.* **108** 068701
[58] Zhang S B, Wei S H and Zunger A 2001 *Phys. Rev.* B **63** 075205
[59] Chandrasekharaiah M S and Margrave J L 1994 *J. Phys. Chem. Ref. Data* **23** 499
[60] Tomaszkiewicz I, Hope G A and O'Hare P A G 1995 *J. Chem. Thermodyn.* **27** 901
[61] Colin R and Drowart J 1964 *Trans. Faraday Soc.* **60** 673
[62] Kittel C 2005 *Introduction to Solid State Physics* 8th edn (Hoboken: Wiley)
[63] Fritze S, Dadgar A, Witte H, Bügler M, Rohrbeck A, Bläsing J, Hoffmann A and Krost A 2012 *Appl. Phys. Lett.* **100** 122104
[64] Zeng H, Duan G, Li Y, Yang S, Xu X and Cai W 2010 *Adv. Funct. Mater.* **20** 561